

ARMY RESEARCH LABORATORY



**Effect of Loading Rate and Orientation on the Compressive
Response of Human Cortical Bone**

by B. Sanborn, C. A. Gunnarsson, M. Foster, P. Moy, and T. Weerasooriya

ARL-TR-6907

May 2014

NOTICES

Disclaimers

The findings in this report are not to be construed as an official Department of the Army position unless so designated by other authorized documents.

Citation of manufacturer's or trade names does not constitute an official endorsement or approval of the use thereof.

Destroy this report when it is no longer needed. Do not return it to the originator.

Army Research Laboratory

Aberdeen Proving Ground, MD 21005-5069

ARL-TR-6907

May 2014

Effect of Loading Rate and Orientation on the Compressive Response of Human Cortical Bone

B. Sanborn and M. Foster
Oak Ridge Institute for Science and Education

C. A. Gunnarsson, P. Moy, and T. Weerasooriya
Weapons and Materials Research Directorate, ARL

REPORT DOCUMENTATION PAGE			<i>Form Approved</i> OMB No. 0704-0188		
Public reporting burden for this collection of information is estimated to average 1 hour per response, including the time for reviewing instructions, searching existing data sources, gathering and maintaining the data needed, and completing and reviewing the collection information. Send comments regarding this burden estimate or any other aspect of this collection of information, including suggestions for reducing the burden, to Department of Defense, Washington Headquarters Services, Directorate for Information Operations and Reports (0704-0188), 1215 Jefferson Davis Highway, Suite 1204, Arlington, VA 22202-4302. Respondents should be aware that notwithstanding any other provision of law, no person shall be subject to any penalty for failing to comply with a collection of information if it does not display a currently valid OMB control number. PLEASE DO NOT RETURN YOUR FORM TO THE ABOVE ADDRESS.					
1. REPORT DATE (DD-MM-YYYY) May 2014		2. REPORT TYPE Final		3. DATES COVERED (From - To) January 2012–January 2013	
4. TITLE AND SUBTITLE Effect of Loading Rate and Orientation on the Compressive Response of Human Cortical Bone			5a. CONTRACT NUMBER		
			5b. GRANT NUMBER		
			5c. PROGRAM ELEMENT NUMBER		
6. AUTHOR(S) B. Sanborn,* C. A. Gunnarsson, M. Foster,* P. Moy, and T. Weerasooriya			5d. PROJECT NUMBER		
			5e. TASK NUMBER		
			5f. WORK UNIT NUMBER		
7. PERFORMING ORGANIZATION NAME(S) AND ADDRESS(ES) U.S. Army Research Laboratory ATTN: RDRL-WMP-B Aberdeen Proving Ground, MD 21005-5069			8. PERFORMING ORGANIZATION REPORT NUMBER ARL-TR-6907		
9. SPONSORING/MONITORING AGENCY NAME(S) AND ADDRESS(ES)			10. SPONSOR/MONITOR'S ACRONYM(S)		
			11. SPONSOR/MONITOR'S REPORT NUMBER(S)		
12. DISTRIBUTION/AVAILABILITY STATEMENT Approved for public release; distribution is unlimited.					
13. SUPPLEMENTARY NOTES *Oak Ridge Institute for Science and Education, 4692 Millennium Drive, Ste. 101, Belcamp, MD 21017					
14. ABSTRACT Under extreme environments, such as a blast or impact event, the human body is subjected to high-rate loading, which results in torn tissues and broken bones. The ability to numerically simulate these high-rate events would improve protective gear by iterating on different protective configurations. Computer codes require input of accurate rate-dependent material models representing the deformation and failure (or injury) to properly predict the response during simulation. Therefore, the high-rate material response must be measured for simulation of high-rate events like blast. In this study, cortical bone compression specimens were extracted from the longitudinal and transverse directions relative to the long axis of the femur from three male donors, ages 36, 43, and 50. The compressive behavior of the cortical bone was studied at quasi-static (0.001/s), intermediate (1/s), and dynamic (1000–2000/s) strain rates using a split-Hopkinson pressure bar to determine the strain rate dependency on the strength of bone. Experimental results indicate that the cortical bone material is anisotropic and stronger in the longitudinal direction compared to the transverse direction. The human cortical bone was also rate dependent in both directions.					
15. SUBJECT TERMS SHPB, cortical bone, compressive response, strain rate					
16. SECURITY CLASSIFICATION OF:			17. LIMITATION OF ABSTRACT UU	18. NUMBER OF PAGES 36	19a. NAME OF RESPONSIBLE PERSON B. Sanborn
a. REPORT Unclassified	b. ABSTRACT Unclassified	c. THIS PAGE Unclassified			19b. TELEPHONE NUMBER (Include area code) 410-306-4925

Contents

List of Figures	iv
List of Tables	iv
Acknowledgments	v
1. Introduction	1
2. Experiments	3
2.1 Material	3
2.2 Quasi-Static and Intermediate Rate Experiments.....	4
2.3 High-Rate Experiments	4
3. Results	11
4. Discussion	14
4.1 Effects of Compression on Cortical Bone	14
4.2 Young's Modulus	18
4.3 Comparison of Mechanical Response of Tibia and Femur	19
5. Conclusions	20
6. References	21
Distribution List	25

List of Figures

Figure 1. Hierarchical structure of cortical bone.	1
Figure 2. Specimens were extracted from the diaphysis.....	4
Figure 3. Raw data from SHPB experiment on human cortical bone.....	5
Figure 4. Dynamic equilibrium of cortical bone compression sample.	6
Figure 5. Strain rate and strain histories of human cortical bone specimen at high rate using bar signals.	7
Figure 6. Typical strain histories from a dynamic (transverse) compression experiment using DIC and bar signal analysis.	8
Figure 7. Strain and load histories for typical high-rate compression experiment.	9
Figure 8. High-rate images of the specimen during the experiment with DIC strain contours at times (a) 36 μ s, (b) 50 μ s, (c) 62 μ s, (d) 74 μ s, (e) 88 μ s (max load), (f) 98 μ s, (g) 104 μ s, (h) 110 μ s, and (i) 148 μ s (fully failed). The length of the speckled bone in the photos is approximately 3–4 mm.....	10
Figure 9. Stress-strain behavior of human femoral cortical bone at multiple loading rates.	12
Figure 10. Failure stress as a function of strain rate.	12
Figure 11. Average Young’s modulus as a function of strain rate.	13
Figure 12. Average strain to failure as a function of strain rate.	14
Figure 13. Compressive strength of cortical bone as a function of strain rate from various human and animal studies.	18

List of Tables

Table 1. Number of experiments in each loading direction for each strain rate.....	4
Table 2. Longitudinally loaded compression results from various studies, including this study at different loading rates.	16
Table 3. Transversely loaded compression results from various studies in literature, including this study at different loading rates.	17

Acknowledgments

The authors would like to acknowledge Mr. Jeff Gair of the Oak Ridge Institute for Science and Education for assistance in the specimen fabrication process and Mr. Ronn Wade and his team at the Maryland State Anatomy Board for assistance in procuring the cadaveric donors for this study.

INTENTIONALLY LEFT BLANK.

1. Introduction

Bone is a complex hierarchical structure organized at a variety of length scales, as shown in figure 1. At the nano scale, cortical bone comprises collagen and hydroxyapatite crystals. At the micro scale, these constituents organize into mineralized collagen fibrils. Fiber arrays are further organized into a lamellar orientation that makes up osteons. These osteons are about 10–500 μm in diameter (1) and are oriented parallel to the longitudinal axis of long bones, such as the femur. The orientation of osteons creates anisotropy that must be understood for numerical modeling efforts. Several studies on bone have been conducted to study the fracture behavior at the micro scale during quasi-static loading (2, 3). The fracture behavior of human bone has also been investigated at a high loading rate (4). Quantification of the anisotropic compressive behavior of bone is critical for building material models. To ultimately understand the response of humans exposed to dynamic loads, high-rate material properties of human tissues, such as bones, are required to obtain valid simulation results. Material models require accurate material properties to properly predict failure during simulation.

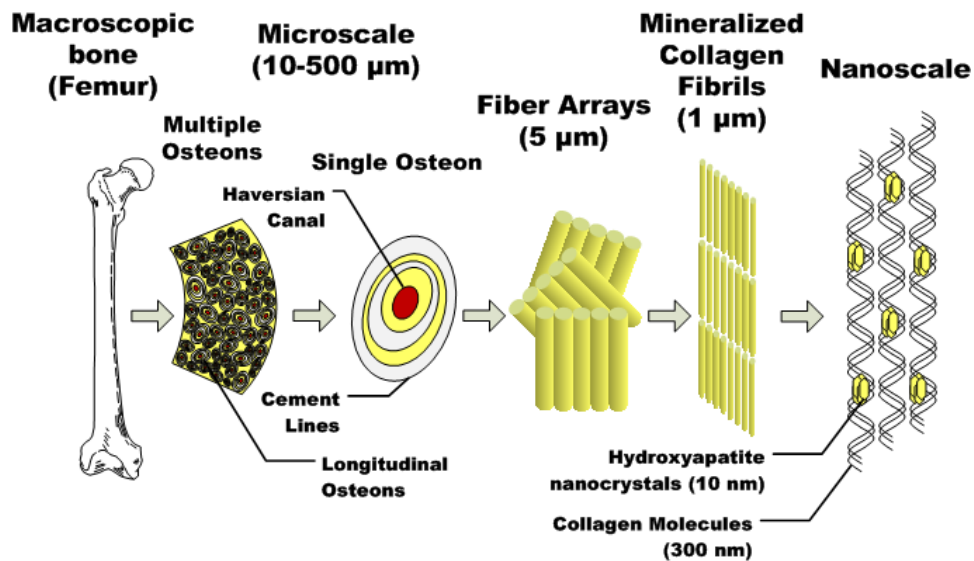


Figure 1. Hierarchical structure of cortical bone.

McElhaney (5) first investigated the strain rate dependence of human cortical bone in compression. These high-rate properties were studied using a piezoelectric load cell and piston arrangement up to strain rates of 1500/s. They found that the bone material was viscoelastic and rate dependent in compression. However, the major caveat of this study is that they used embalmed bone. Others have shown that the ultimate strength, maximum strain, and modulus of elasticity measurements do not represent the actual bone response (6), and the length of the formalin concentration affects bone material properties (7). The aim of the current study is to fill this gap by examining the material properties of bones that had not been embalmed.

The split-Hopkinson pressure bar (SHPB) experimental method has been used to study the rate dependence of primarily animal cortical bone. Tennyson et al. (8) studied specimens from bovine femurs subjected to a range of strain rates from 10 to 450/s and provided a linear viscoelastic model describing the mechanical behavior. Stress and strain measurements were computed using typical SHPB wave mechanics. Lewis and Goldsmith (9, 10) developed a biaxial method to test bovine bone samples under simultaneous compression and torsion, and also under compression, tension, and torsion separately. Importantly, they used strain gages bonded directly to the surface of the bone specimens for more accurate strain measurements compared to previous work (8). They found that the prefracture response in compression was viscoelastic, and the compressive response increased with strain rate. Additionally, the bone accumulated residual plastic strain after load removal prior to fracture in combined torsion and compression. This was not the case in uniaxial compression.

A drawback of the strain gage technique is that the fresh bone specimens needed to be dried out for 2 full days for proper strain gage adhesion. This drying process alters the mechanical response of the bone because of the hydration-dependent behavior of collagen in the bone (11, 12). Katsamanis and Raftopoulos (13) studied the effect of loading rate on the Young's modulus and Poisson's ratio of human femoral cortical bone using one-dimensional wave theory and strain gages bonded to the surface of the bone in two directions at multiple locations. The experiments were conducted by impacting small steel balls longitudinally on the bone specimens. The Young's modulus of the bone increased from 16.2 GPa at quasi-static rates to 19.9 GPa at dynamic rates. None of these studies investigated the mechanical response associated with the inherent strong microstructural anisotropy of the bone.

Tanabe et al. (14) studied anisotropy of bovine femur and the effect of strain rate up to 100/s. The elastic modulus was found to be strongly dependent on the loading orientation of the bone with the elastic modulus being the greatest in the longitudinal direction. The value of the elastic modulus of the transversely oriented specimens was less than half that of the longitudinal specimens. No difference in elastic modulus was found for specimens taken from the radial or tangential directions of the transverse cortical bone. Adharapurapu et al. (15) investigated the fracture toughness properties and the rate-dependent compressive behavior of bovine cortical bone taken from the longitudinal and transverse directions of the bone axis. Similar to what was previously reported, the bone was found to be anisotropic. The longitudinally oriented specimens were about 50% stronger than the transversely oriented specimens under the same experimental conditions. Both the strength and stiffness of the bovine bone increased from quasi-static to high loading rate, while the elongation decreased.

In contrast, Ferreira et al. (16) also studied bovine cortical bone at high strain rate using an SHPB apparatus and did not find statistically different results concerning the compressive strength of the longitudinal or transverse specimens from the bovine bone. One possible reason for this difference is that they did not ensure that their specimens were in dynamic equilibrium or at a constant strain rate. Lee and Park (17) found qualitative evidence of anisotropy, which is in

agreement with Adharapurapu et al. (15) using the SHPB technique; however, their experiments suffered from problems with specimen dynamic equilibrium and bar alignment issues, as outlined by Chen and Song (18). Similarly, Kulin et al. (19) studied the effect of loading rate and age on the failure behavior of equine cortical bone and found it to be strain rate dependent and anisotropic. Like the bovine results, equine cortical samples taken from the longitudinal direction were both stronger and stiffer at all loading rates compared to transverse specimens. Porcine cortical bone has also been investigated at high rates (20, 21).

The microstructure of human bone is Haversian, whereas the microstructure of porcine and bovine bones possibly has a plexiform structure (14, 22, 23). Plexiform bone is typically found in animals that grow at a fast rate (22). Parts of bovine femur may have a Haversian microstructure, while other parts may have a plexiform structure. Since plexiform bone is rarely found in humans, dynamic mechanical behavior obtained through experimentation on animal bones should not be used in numerical models that are used to simulate the damage to human bones during high loading rate events.

Aside from the work of Lewis and Goldsmith (9, 10), previous works (15, 17, 19) all used traditional SHPB assumptions to calculate the failure strain of the specimen. Bone fails at relatively small strains and does so in a linear fashion similar to brittle materials, such as ceramics. This small strain to failure makes measuring the deformation of the specimen using bar signals extremely difficult (18). To avoid making inaccurate measurements of failure strains using SHPB bar signals, a noncontact digital image correlation (DIC) method was used in this study to measure the failure strain of the material at all loading rates. Furthermore, this study is the first to investigate the mechanical response of undried, unembalmed human femoral cortical bone in two directions at multiple loading rates under dynamic equilibrium and constant strain rate conditions.

2. Experiments

2.1 Material

Cortical bone samples were extracted from the femur diaphysis (shown in figure 2) of three male cadavers, ages 36, 43, and 50. Samples were extracted from the anterior, posterior, medial, and lateral regions along the femur diaphysis. The location of each specimen was carefully recorded. Nominal dimensions of the cube-shaped samples were $3 \times 3.25 \times 4$ mm. The gage lengths of the longitudinal and transverse specimens were 3.22 ± 0.08 mm and 2.96 ± 0.125 mm, respectively. The cortical bone samples were stored in Hank's Buffered Salt Solution after fabrication and prior to testing to preserve mechanical properties (24). A total of 71 experiments were conducted for samples taken from directions longitudinal and transverse to the osteon direction in the bone. Table 1 shows the breakdown of the number of individual samples used at each loading rate and direction. Roughly the same number of samples from each donor at each rate was used to obtain an average behavior of cortical bone in uniaxial compression.

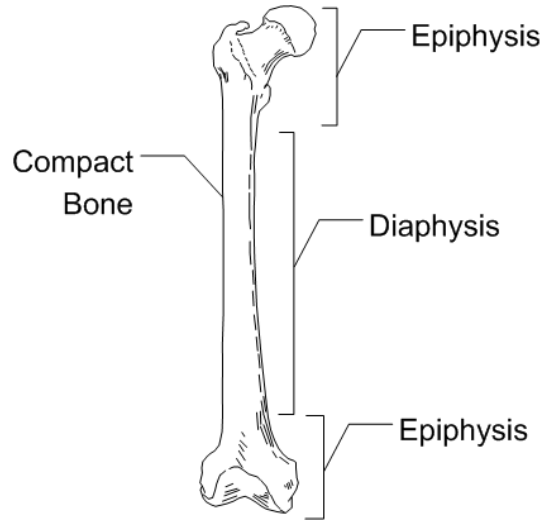


Figure 2. Specimens were extracted from the diaphysis.

Table 1. Number of experiments in each loading direction for each strain rate.

Rate	Transverse Direction	Longitudinal Direction
Quasi-static (~0.001/s)	12	12
Intermediate (~1/s)	11	11
High (~1000/s)	14	11

2.2 Quasi-Static and Intermediate Rate Experiments

An Instron load frame in displacement control was used for quasi-static (approximately 0.001/s) and intermediate (approximately 1/s) rate experiments. Typically for brittle materials, such as ceramics and bone, strain calculations are made using strain gages bonded to the surface of the material to extract an accurate strain history of the specimen. In this study, the strain behavior of the bone material was collected using a variety of digital cameras using a DIC method (25–28). This technique avoids problems such as alignment of the gage and other limiting factors such as the maximum strain limit of the strain gage itself. In the DIC technique, a black speckle pattern is applied to a white background on the specimen surface. The DIC software tracks the pixel gray level values of the speckle pattern throughout the experiment and uses relative motion of different points to determine deformation, and therefore strain, on the surface of the specimen. For bone specimens a light mist of matte black paint was applied to the already light color of the bone to create the speckle pattern.

2.3 High-Rate Experiments

High-rate compression experiments were conducted using an SHPB setup. The setup used a solid 19.05-mm incident bar with resistive strain gages and a hollow transmission bar with an outer diameter of 19.05 mm and an inner diameter of 16.17 mm with semiconductor strain gages to improve the quality of the transmitted signal. The engineering stress σ_e is calculated using (18)

$$\sigma_e = \frac{A_t}{A_s} E \varepsilon_t \quad (1)$$

where A_t and A_s are the areas of the transmission bar and specimen, respectively. E is the Young's modulus of the bar material, while ε_t is the strain measured from the transmission bar. Since a hollow transmission bar was used, the strain rate is calculated using (29)

$$\dot{\varepsilon} = \frac{c_0}{L_s} \left[\left(1 - \frac{A_i}{A_t}\right) \varepsilon_i(t) - \left(1 + \frac{A_i}{A_t}\right) \varepsilon_r(t) \right] \quad (2)$$

where c_0 is the wave speed of the bar material and L_s is the length of the sample. A_i and A_t are the cross-sectional areas of the incident and transmission bars, respectively. The quantities ε_i and ε_r are the incident and reflected signals in the incident bar. The engineering strain is obtained from the time integration of the bar signals in equation 2. However, just as in the quasi-static and intermediate rate cases, it is difficult to accurately measure strains in brittle materials. Hence, DIC was also used to obtain the strain history of the specimen at high loading rate.

A typical example of the raw strain gage signals from the SHPB experiment on bone is shown in figure 3. A triangular-shaped incident pulse, such as the one shown in figure 3, is typically used for high-rate experiments on brittle materials (18). Pulse shaping was used to vary the rise time to ensure that the bone specimen was in dynamic equilibrium over the course of the experiment. Verification of the dynamic equilibrium requires that the forces on either side of the specimen stay constant throughout the experiment, or $F_{\text{front}} = F_{\text{back}}$. The typical measured or derived forces on either side of the specimen, shown in figure 4, verify that the front and back end forces were the same throughout the experiment. The force history calculated using the incident and reflected signals is noisier than the transmission force history because of the higher signal-to-noise ratio of the hollow transmission bar compared to the solid incident bar, as well as the semiconductor gages used on the transmission bar compared to the resistive gages used on the incident bar.

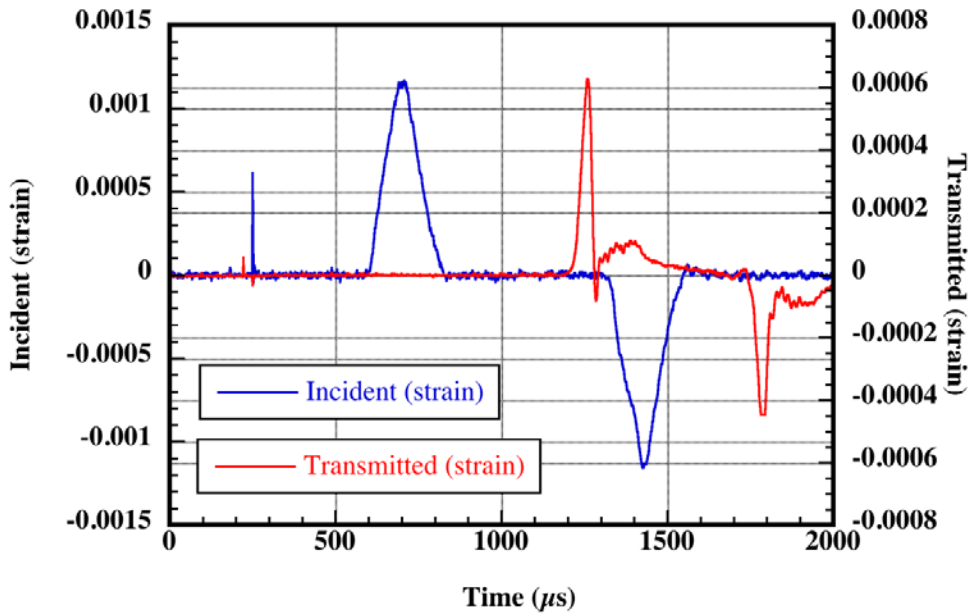


Figure 3. Raw data from SHPB experiment on human cortical bone.

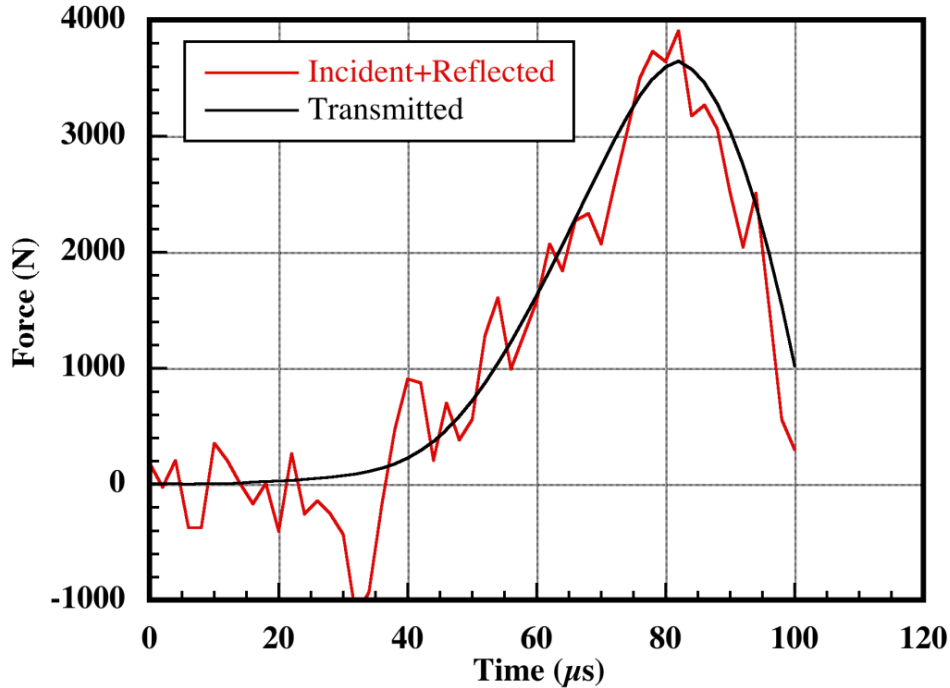


Figure 4. Dynamic equilibrium of cortical bone compression sample.

In addition to being in dynamic equilibrium, the cortical bone specimen experienced an approximately constant strain rate of deformation after initial ramp loading, as shown in a typical strain and strain rate histories in figure 5. The curve in figure 5 shows that after a strain acceleration time of about 30–40 μs , the sample deformed at an approximate strain rate between 1700 and 2000/s until about 80 μs . The strain history also becomes approximately linear from 40 to 80 μs , after the 30- to 40- μs rise time. The strain rate behavior shown in figure 4 follows the work by Frew et al. (30) on brittle materials, such as Macor and Indiana limestone. After 80 μs , the specimen begins to fail with catastrophic damage. After initiation of the catastrophic damage, there is little resistance to the motion of the incident bar, so the increase in the strain rate curve past 80 μs is not a valid representation of the strain rate in the specimen. For this reason, the strain rate history of the bone specimen in this case is no longer applicable after the initiation of the catastrophic failure at 80 μs .

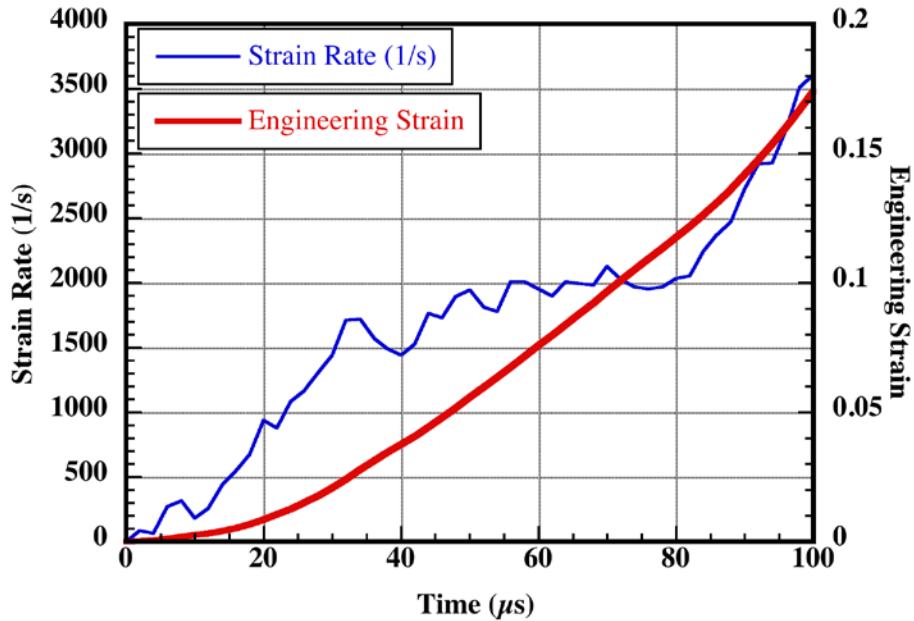


Figure 5. Strain rate and strain histories of human cortical bone specimen at high rate using bar signals.

Measurement of small displacements of the bar ends is inaccurate because of slight variations in strain gage factor and the inability to prepare perfectly flat and parallel loading surfaces. This is why elastic behavior is not reported for most materials using only bar signals—directly bonded strain gages or other optical techniques are necessary to accurately obtain the small strain behavior. In this study, DIC was used to make strain and strain rate measurements. The strain history was extracted using DIC in addition to standard SHPB bar signal analysis, as shown in figure 6. In figure 6, the DIC strain values are lower than the strain as calculated using the bar signals. The DIC data include both the maximum values and average values. The maximum and average DIC strain values are nearly identical up to the maximum load occurring at 90 μs into the experiment. This indicates that the strain profile over the specimen is relatively uniform. The two curves diverge after maximum load is attained as the specimen begins to crack or fail and develops localized strain concentrations.

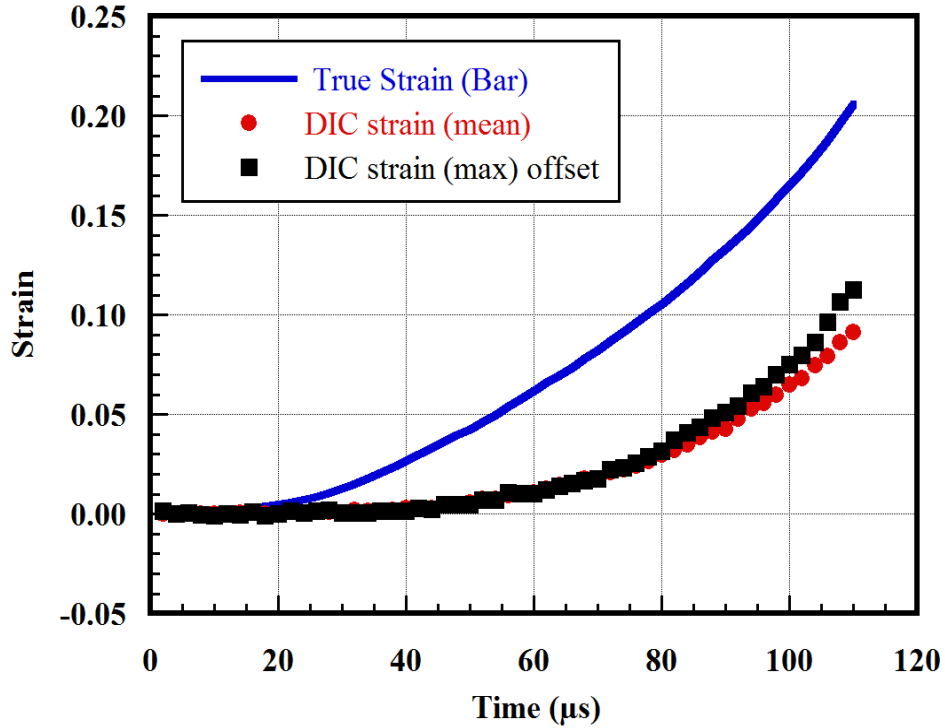


Figure 6. Typical strain histories from a dynamic (transverse) compression experiment using DIC and bar signal analysis.

The load and averaged DIC strain histories for the same experiment are shown in figure 6. As is shown in figure 7, the strain history is not linear up to the max load during the experiment; however, the strain is approximately linear from half load (50 μs) to max load (90 μs). This indicates that the strain rate is approximately constant over the latter half of the experiment. It is over this time range that the strain history was used to determine the strain rate of the experiment. For this experiment, the strain rate was approximately 960/s. After maximum load is reached, the specimen begins to fail and the strain rate increases.

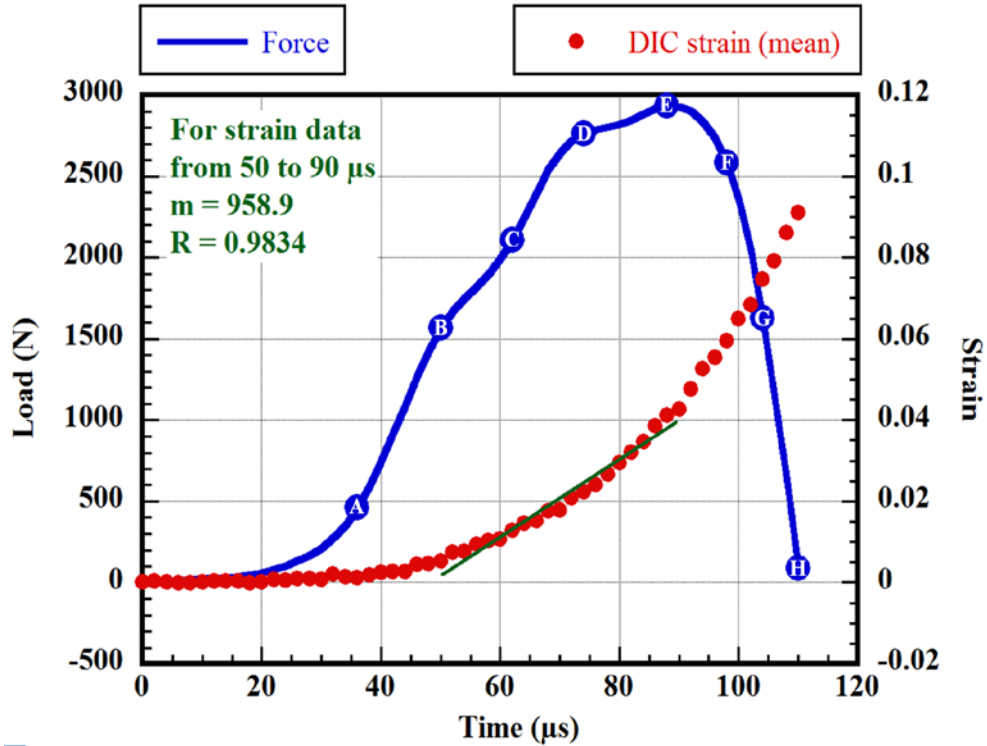


Figure 7. Strain and load histories for typical high-rate compression experiment.

The high-rate compression experiments were performed with 19.05-mm-diameter bars. The large diameter of the bars created blurred edges in the high-speed imaging due to the bar surface being closer to the optical lens than the focal plane. This limited the amount of axial length of the specimen that was available to be used in the DIC analysis to obtain strain measurements. Smaller diameter bars, such as 12.7 mm or even 6.35 mm, would reduce the blurriness since the bar surfaces would be closer to the focal plane of the camera and produce images with a larger area of interest for DIC analysis. Though this narrow area was used to obtain strain measurements, the strain is uniform across the surface of the specimen within this area, indicating the validity of the DIC strain measurement method. Figure 8 shows a series of images of this compression specimen with axial-strain contours, during the high-rate experiment. The eight images (a–h) correspond to the blue point-markers on the load history in figure 7. Figure 8i shows the specimen after failure (no contour is present because the DIC analysis was unusable). The strain contours in figure 8 show that after the maximum load is reached (e), strain begins to localize, leading to failure. Therefore, the strain given in figure 7 after maximum load is the averaged strain in the specimen, although there are points of higher strain due to nonuniform localized deformation (see figure 6 for a comparison between averaged and maximum strain after peak load).

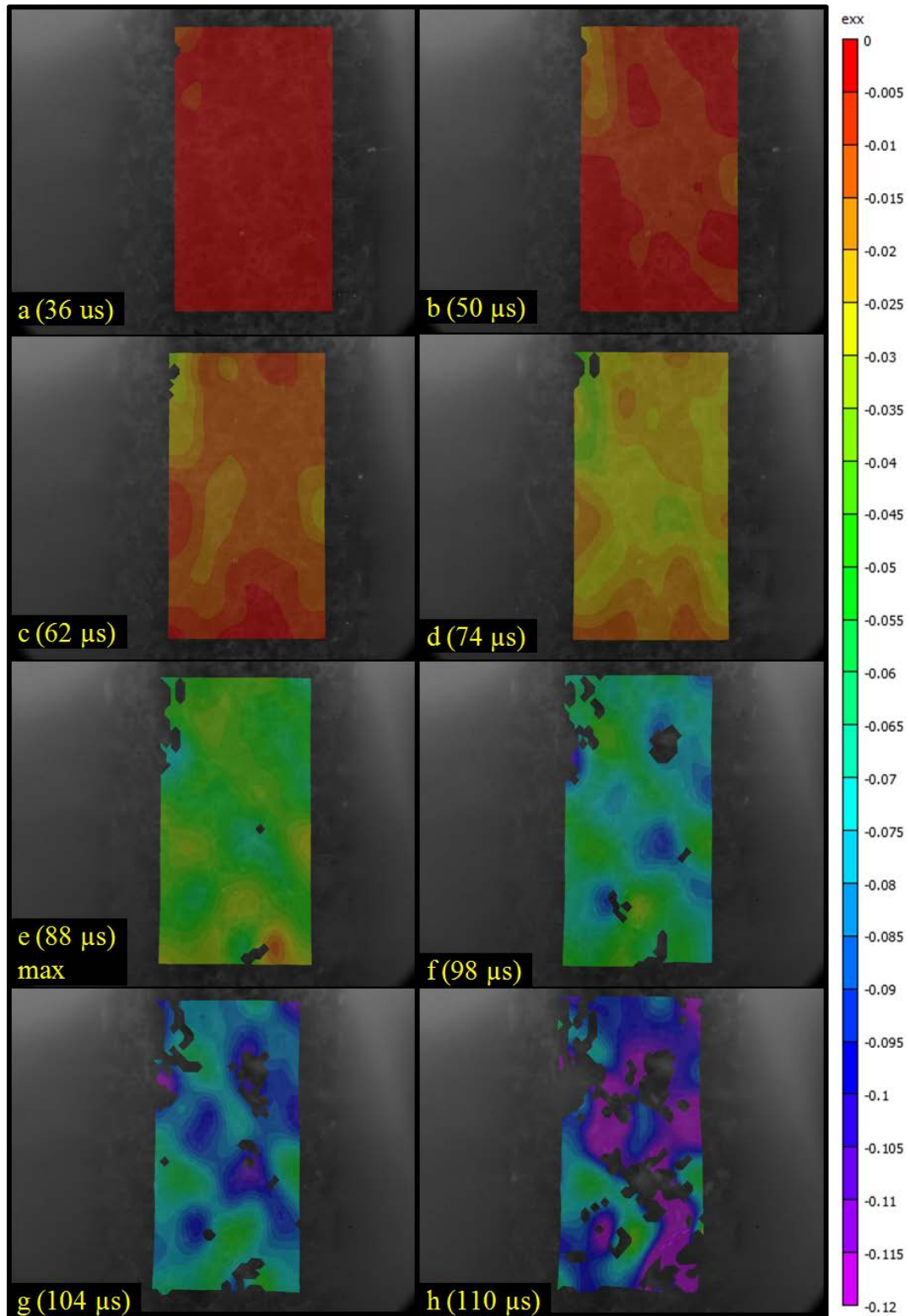


Figure 8. High-rate images of the specimen during the experiment with DIC strain contours at times (a) 36 μ s, (b) 50 μ s, (c) 62 μ s, (d) 74 μ s, (e) 88 μ s (max load), (f) 98 μ s, (g) 104 μ s, (h) 110 μ s, and (i) 148 μ s (fully failed). The length of the speckled bone in the photos is approximately 3–4 mm.

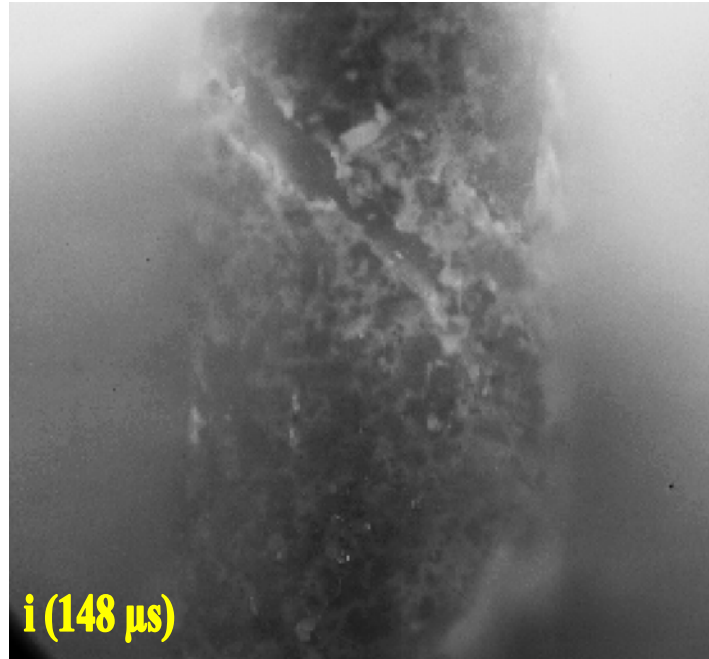


Figure 8. High-rate images of the specimen during the experiment with DIC strain contours at times (a) 36 μs , (b) 50 μs , (c) 62 μs , (d) 74 μs , (e) 88 μs (max load), (f) 98 μs , (g) 104 μs , (h) 110 μs , and (i) 148 μs (fully failed). The length of the speckled bone in the photos is approximately 3–4 mm (continued).

3. Results

The stress-strain response from quasi-static, intermediate, and high-rate experiments are shown in figure 9. Error bars in all plots represent ± 1 standard deviation. The ultimate strength was found to be dependent on the strain rate; the strength increased as the strain rate increased for both orientations. This relationship is linear when plotted on a semi-log scale, as shown in figure 10, meaning that the true relationship is exponential. Failure strength was also dependent on the loading direction of the specimen relative to the long axis of the bone. Longitudinally loaded specimens failed at a higher strength compared to transversely loaded specimens for the same strain rate. The results show a high amount of scatter, which is not surprising because of the nature of biological materials. This variability is most likely due to the large number of natural differences in the bone, including mineral content, microstructural flaws, and the variation in the osteon size or the orientation relative to the loading direction. Specimen location dependency (relative to location in the diaphysis or angular position) was not investigated for this small set of specimen extraction locations, despite extracting specimens from anterior, posterior, medial, and lateral locations along the shaft of the diaphysis. Conclusions regarding any correlation between age and compressive strength could not be made because of both the limited number of donors and the narrow age range used in this study.

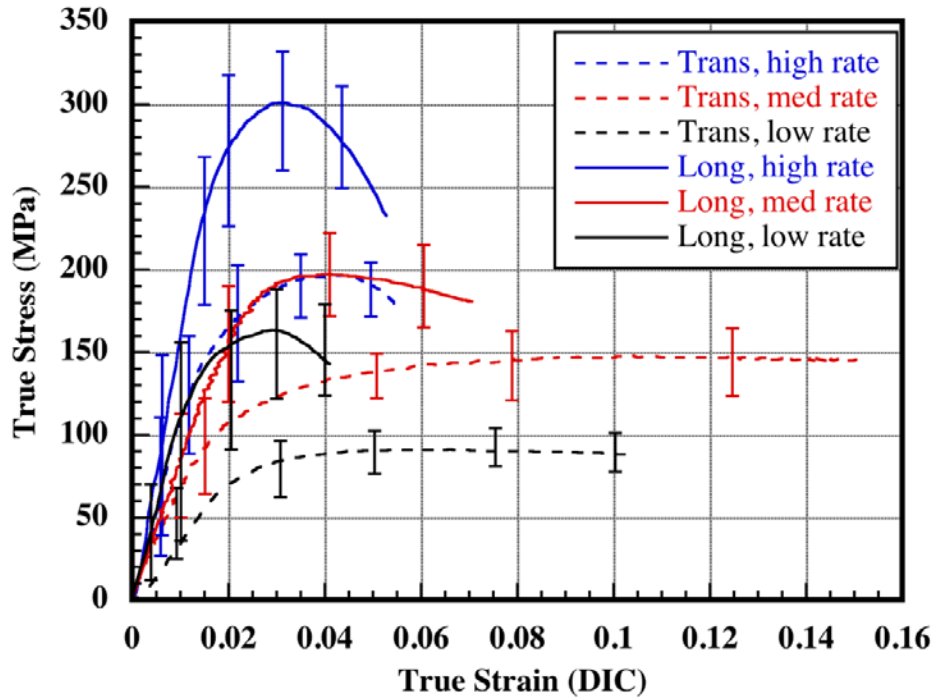


Figure 9. Stress-strain behavior of human femoral cortical bone at multiple loading rates.

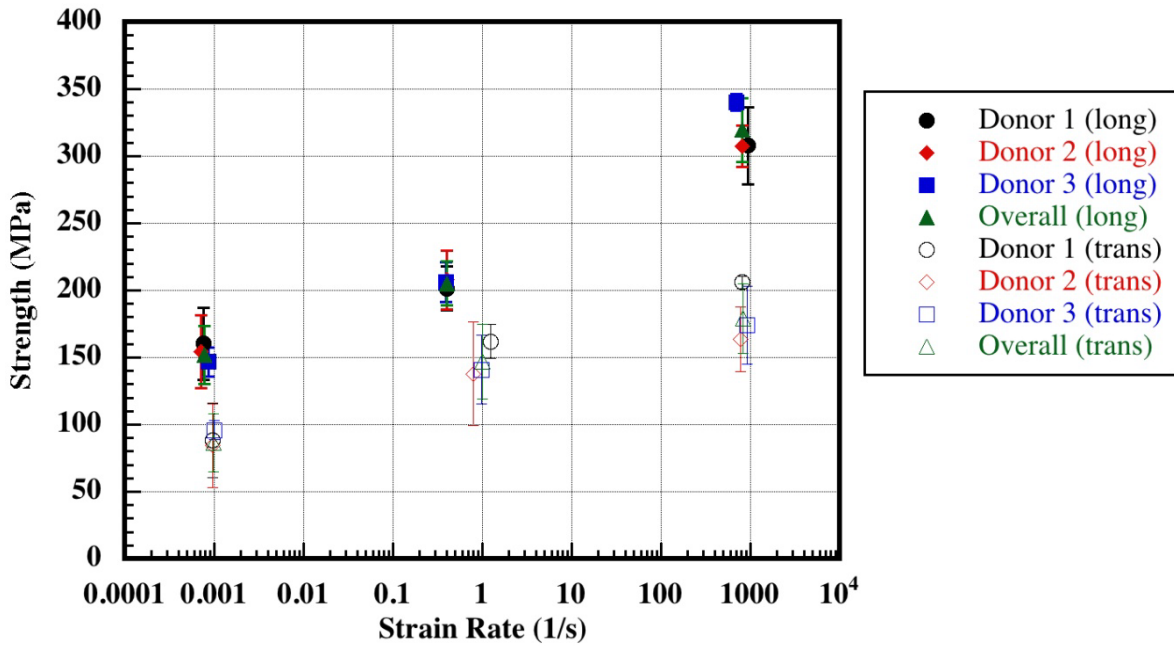


Figure 10. Failure stress as a function of strain rate.

In addition to failure strength, the Young's modulus was also loading rate dependent, as shown in figure 11. The average Young's modulus of both the longitudinal and transverse samples increased linearly with strain rate when plotted on a semi-log scale, indicating an exponential behavior. The average Young's modulus behavior also depended on specimen loading direction. Longitudinally loaded specimens were stiffer than transversely loaded specimens.

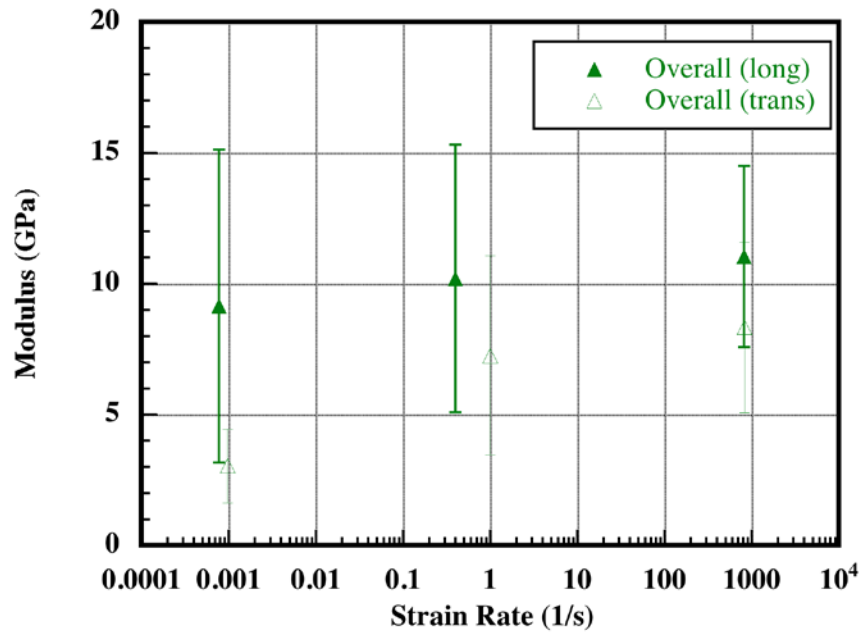


Figure 11. Average Young's modulus as a function of strain rate.

A summary of ultimate strain (strain at the maximum stress level) as a function of strain rate is shown in figure 12. The transversely loaded specimens reached a higher ultimate strain compared to the longitudinally loaded specimens at low and intermediate rates; however, at high rate the failure strains of the two directions approached the same range.

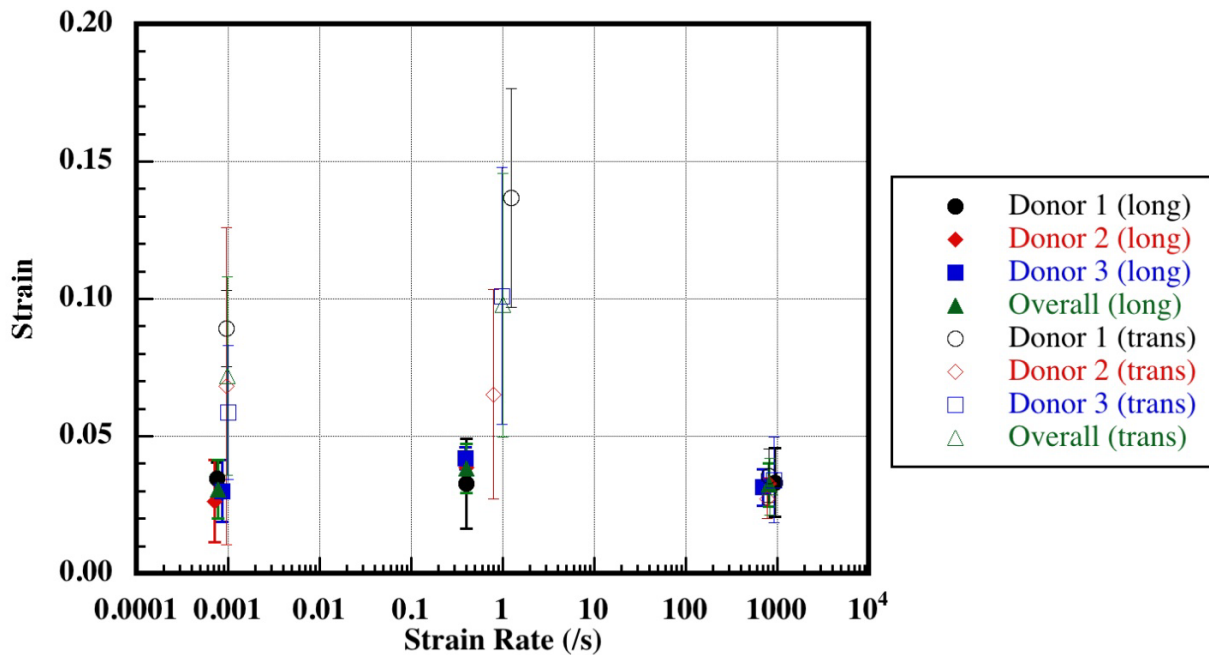


Figure 12. Average strain to failure as a function of strain rate.

4. Discussion

4.1 Effects of Compression on Cortical Bone

A uniaxial compressive study of human femoral cortical bone was completed over a range of strain rates from quasi-static (0.001/s) to high rates (approximately 1000/s). Loading was applied in the transverse and longitudinal directions of the bone axis. An Instron load frame was used for quasi-static and intermediate rate experiments, while an SHPB setup was used for high-rate investigations. Optical strain measurements with a DIC method were used to measure strain. The mechanical properties of the bone used in this study were found to be anisotropic; the measured properties in the longitudinal direction were higher than the transverse direction. The ultimate strength of the bone material varied from 152.1 ± 21.6 MPa at quasi-static rate to 319 ± 23.9 MPa at high rate in the longitudinal direction and the transverse strength was 86.6 ± 21.7 MPa at quasi-static rate and 178.9 ± 26.02 MPa at dynamic rates.

The compressive stress-strain response found in this study agreed with other studies on human bones. McElhaney (5) found that an embalmed human femur had an ultimate strength of about 140 MPa at quasi-static rate, while the strength at high rate (1500/s) was about 300 MPa in the longitudinal direction of the bone. In general, direct comparisons between embalmed and fresh bone are unwise because of the significant effects of embalming on bone microstructure and constituents leading to altered ultimate strength, failure strain, and modulus of elasticity of bone

material (6). In an attempt to quantify these effects, McElhaney et al. (6) conducted a comparative study and found that embalming caused a 12% reduction in ultimate compressive strength. The value of ultimate strength found in this study on fresh bone was 152.1 ± 21.6 MPa at quasi-static and 319 ± 23.9 MPa at dynamic rate in the longitudinal direction. After the 12% reduction in strength was accounted for, the range of ultimate strength found for human bone by McElhaney (5) would be 168–355 MPa, which are similar to the values found in this study.

Reilly and Burstein's (22) quasi-static results of longitudinally loaded compression experiments on human femur agree with the response obtained in this study, having a value of 187 MPa. The compressive response for the transverse direction, however, was found to be 132 MPa at a quasi-static rate (22), while an average value of 86.6 MPa was recorded in this study. A comprehensive table containing the mechanical response from this study and various other studies is shown in tables 2 and 3. Like human bone, Adharapurapu et al. (15) also found that bovine bone was rate dependent in compression and also showed a linear dependence with strain rate when plotted in a semi-log plot. Quantitatively, bovine and equine bones displayed higher ultimate stresses compared to the human bones used in this study, underscoring the necessity for human tissue studies at high strain rates relevant to extreme dynamic environments when developing material response models to be incorporated into numerical simulations. In addition, figure 13 graphically shows the compressive strengths of several studies as a function of strain rate. The divergence of animal data from human data at a high rate can be appreciated. At high loading rates, the compressive strength of animal cortical bone is much higher than the corresponding compressive strength in human cortical bone.

The overall stress-strain trends of cortical bone found in this study agree with other studies on animal bones and observed that the mechanical properties of the bone were anisotropic; the measured properties in the longitudinal direction were higher than the transverse direction. Kulin et al. (19) found that wet equine bone was anisotropic and loading rate dependent when loaded in both the longitudinal and transverse directions. Adharapurapu et al. (15) also observed an anisotropic compressive response in wet cortical bovine specimens. Unfortunately, some investigators used dry bones for their studies, making it impractical to draw comparisons of the mechanical response obtained to wet bones because of the significant effect from hydration and collagen on the mechanical behavior (11, 12).

Table 2. Longitudinally loaded compression results from various studies, including this study at different loading rates.

Study	Material	Test Type	Age (years)	Strain Rate (1/s)	Compressive Strength (MPa)	Elastic Modulus (GPa)	Strain to Failure (%)	Strain Measurement Method
(31)	Femur	Low strain rate	—	—	—	17.3	—	—
(32)		Bending	—	—	—	15.8	—	—
(5)	Femur (embalmed)	Longitudinal compression	24 male	0.001	150.34	15.17	1.65	Piston velocity
(5)	Femur (embalmed)	Longitudinal compression	25 male	0.01	179.31	17.24	1.75	Piston velocity
(5)	Femur (embalmed)	Longitudinal compression	26 male	0.1	200.0	17.93	1.8	Piston velocity
(5)	Femur (embalmed)	Longitudinal compression	27 male	1	220.69	22.07	1.78	Piston velocity
(5)	Femur (embalmed)	Longitudinal compression	28 male	300	279.31	29.66	1.1	Piston velocity
(5)	Femur (embalmed)	Longitudinal compression	29 male	1500	317.24	40.69	0.95	Piston velocity
(33)	—	Ultrasonics	—	—	—	29.5	—	—
(34)	Femur	Hydrated	23 male	0.052	—	15.94 ± 0.4	—	Strain gage
(34)	Femur	Dry	23 male	0.052	—	18.91 ± 0.3	—	Strain gage
(22)	Femur	Longitudinal compression, wet	21 male	0.2–0.5	206 ± 10	—	1.9 ± 0.29	Extensometer
(22)	Femur	Longitudinal compression, wet	22 male	0.2–0.5	211 ± 14.4	—	1.8 ± 0.07	Extensometer
(22)	Femur	Longitudinal compression, wet	31 male	0.2–0.5	203 ± 27.6	—	1.9 ± 0.34	Extensometer
(22)	Femur	Longitudinal compression, wet	52 male	0.2–0.5	198 ± 12.7	—	1.8 ± 0.38	Extensometer
(22)	Femur	Longitudinal compression, wet	Average	0.2–0.5	193	—	—	—
(35)	Femur	—	20–29 M&F	Low	209 ± 3.5	18.1 ± 0.28	—	Extensometer
(35)		—	30–39 M&F	Low	209 ± 8.5	18.6 ± 0.14	—	Extensometer
(35)		—	40–49 M&F	Low	200 ± 17.0	18.7 ± 1.48	—	Extensometer
(35)		—	50–59 M&F	Low	192 ± 16.8	18.2 ± 0.61	—	Extensometer
(35)		—	60–69 M&F	Low	179 ± 14.9	15.9 ± 0.68	—	Extensometer
(35)		—	70–79 M&F	Low	190 ± 19.6	18.0 ± 1.86	—	Extensometer
(35)		—	80–89 M&F	Low	180	15.4	—	Extensometer
(35)	Tibia	—	30–39 M&F	Low	204	35.3	—	Extensometer
(35)		—	40–49 M&F	Low	204 ± 7.6	30.6 ± 11.05	—	Extensometer
(35)		—	50–59 M&F	Low	192 ± 0.5	24.5 ± 1.05	—	Extensometer
(35)		—	60–69 M&F	Low	183 ± 6.0	25.1 ± 1.12	—	Extensometer
(35)		—	70–79 M&F	Low	183	26.7	—	Extensometer
(35)		—	80–89 M&F	Low	197	25.9	—	Extensometer

Table 2. Longitudinally loaded compression results from various studies, including this study at different loading rates (continued).

(36)	Femur	—	18–87 M&F	0.001	61.6 ± 4.9	—	—	—
(37)	Femur	Ultrasonics (wet)	—	—	—	5.5	—	—
(13)	Femur	Dry, ball bearing impact	—	0.00002	—	16.2	—	Strain gage
(13)	Femur	Dry, ball bearing impact	—	100	—	19.9	—	Strain gage
(38)	Femur or Tibia	Longitudinal compression	4–15	0.1	104	12.47	2.31	Extensometer
(38)	Femur or Tibia	Longitudinal compression	22–61	0.1	194.4	17.7	1.84	Extensometer
This study	Femur	Longitudinal compression	36–50	0.001	152.1 ± 21.6	9.15 ± 5.98	3.06 ± 1.06	DIC (optical)
This study	Femur	Longitudinal compression	36–50	1	205.3 ± 16.5	10.2 ± 5.11	3.83 ± 0.9	DIC (optical)
This study	Femur	Longitudinal compression	36–50	1000	319 ± 23.9	11.05 ± 3.46	3.24 ± 0.79	DIC (optical)

Table 3. Transversely loaded compression results from various studies in literature, including this study at different loading rates.

Study	Material	Test Type	Age (years)	Strain Rate (1/s)	Compressive Strength (MPa)	Elastic Modulus (GPa)	Strain to Failure (%)	Strain Measurement Method
(22)	Femur	Transverse Compression, wet	31 Male	0.2–0.5	151 ± 12.7	—	8.7 ± 2.48	Extensometer
(22)	—	Transverse Compression, wet	52 Male	0.2–0.5	118 ± 13.6	—	2.8 ± 0.29	Extensometer
(22)	—	—	Overall Average	—	133	—	—	—
This Study	Femur	Transverse Compression	36–50	0.001	86.60 ± 21.7	3.05 ± 1.14	7.21 ± 3.61	DIC (optical)
This Study	Femur	Transverse Compression	36–50	1	146.98 ± 27.53	7.24 ± 3.8	9.78 ± 4.79	DIC (optical)
This Study	Femur	Transverse Compression	36–50	1000	178.90 ± 26.02	8.30 ± 3.25	3.17 ± 1.28	DIC (optical)

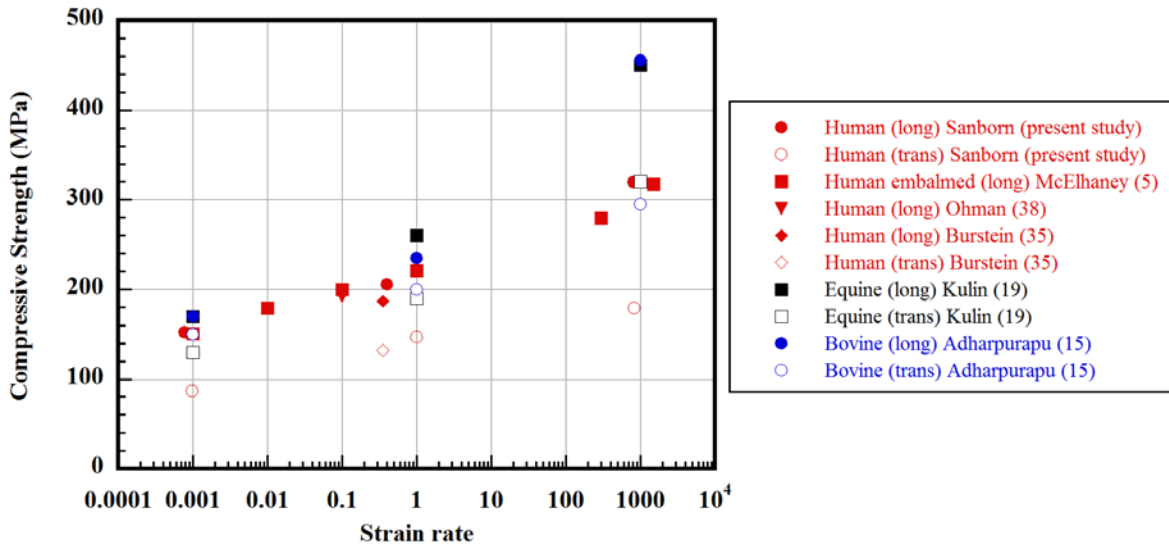


Figure 13. Compressive strength of cortical bone as a function of strain rate from various human and animal studies.

4.2 Young's Modulus

The Young's modulus from this study largely disagreed with moduli measured from other studies. The Young's modulus of the bone in the longitudinal direction was 9.15 ± 5.98 GPa at quasi-static rates, while at dynamic rates the modulus was 11.05 ± 3.46 GPa. In the transverse direction, the Young's modulus of the bone was 3.05 ± 1.14 GPa at quasi-static rate and 8.3 ± 3.25 GPa at high rate, averaging over the three donors. Reilly and Burstein (22) observed an orientation dependence on the modulus of cortical bone at a quasi-static rate; the longitudinal modulus was 17.0 GPa, and the transverse modulus was 11.5 GPa. Ohman et al. (38) investigated the longitudinal compressive behavior of femur and tibia, and through a combined average found a compressive modulus of 17.7 GPa. The strain rate dependence on modulus in the current study also differed from published dynamic data. Katsimanis and Raftopolus (13) also studied the rate-dependent Young's modulus of human femoral cortical bone in the longitudinal direction and found values of 16.2 and 19.9 GPa at quasi-static and dynamic rates, respectively. A possible cause for this difference could be that Katsimanis and Raftopolus (13) used strain gages bonded to the surface of the bone, which included a 2-day drying period of the bones for strain gages to adhere to the surface. Despite this difference in Young's modulus, the rate of increase in modulus with strain rate was similar. The results of Katsimanis and Raftopolus (13) show a 23% increase in modulus from quasi-static to dynamic rates, while our results show an increase of 21% over a similar range of strain rates.

Differences in the measured modulus could be due to preservation methods and moisture content of the specimens; several other investigators dried bone specimens for an extended period of time, which could have affected the measured stiffness. Choi et al. (39) investigated the modulus

of human cortical bone from a tibia using a three-point bend arrangement and found a specimen size dependency on modulus. Specifically, the modulus for relatively large specimens defined as having a height larger than 500 μm was consistently found to be around 15 GPa. Once the specimen size decreased below 500 μm , the modulus dropped to 4.6–5.5 GPa for cortical bone, showing the influence of specimen microstructural effects. Choi et al. (39) posited that the reduction in modulus is due to microstructural defects present in the bone. Essentially, as the specimen size drops and the size of the defects remains constant, defects have a more profound effect on the measured modulus.

4.3 Comparison of Mechanical Response of Tibia and Femur

The mechanical properties of the femur may not represent the mechanical behavior of other bones in the leg. The compressive results from the present study seem to agree with Ohman et al. (38), who found the compressive strength of an adult bone to be 191.4 MPa. However, Ohman et al. (38) mixed femur and tibia specimens and presented them as a single average value.

Furthermore, a study comparing tibia bone material properties to those of the femur found a similar range of values for the ultimate strength at low strain rates (35). However, the stiffness of the tibia was noted to be 34%–90% higher than the stiffness of femur material, concluding that the mechanical properties of the femur and tibia are different and should not be grouped together as one material. This finding was consistent with similar comparison studies on the mechanical properties of the femur and tibia (31, 40, 41). Burstein et al. (35) also showed that femoral tissue undergoes degradation in all mechanical properties with age, while tibial tissue only shows an increase in ultimate strain.

The mechanical properties of various bones differ not only throughout the body, but also within any given bone (42, 43). Studies of the mechanical properties show that the properties of the subchondral bone of the femoral head (44) (the metaphyseal section), which is located between the diaphysis and the epiphysis in the proximal femur, are different from the properties of the diaphysis (45). Regarding the tibia bone, the metaphyseal (46) and subchondral (39) bones in the proximal tibia have been shown to have properties of lower magnitude in comparison to the diaphyseal bone. Because of the differences in the mechanical properties of the femur and tibia, the use of a single value of yield strength, ultimate strength, or modulus for femur and tibia would be inappropriate. Therefore, when developing a high-fidelity computational model of a human anatomy, each type of bone must be studied separately to obtain its specific properties.

Any correlations based on the specimen harvest location could not be concluded from this study with the limited sampling size, even though differences in strength, moduli, and hardness have been shown to vary with specimen location along the femur shaft (diaphysis) as well as at the ends (epiphysis). Conclusions about the relationship of age to ultimate compressive strength or stiffness could not be made because of the narrow age range of the donors in this study.

5. Conclusions

The failure strength of the human cortical bone in two directions was found to be positively correlated with strain rate. These experiments indicate that cortical bone from the human femur shaft is anisotropic, having higher stiffness and strength in the longitudinal direction of the bone at all strain rates. A review of available cortical bone failure strengths indicates that unembalmed and hydrated bone must be studied to obtain an accurate mechanical response. Furthermore, mechanical properties of the femur should not be applied to other bones for numerical modeling purposes, especially in the case of the tibia, which has been found to possess different failure strengths and moduli compared to the femur. Further work is needed to quantify rate-dependent regional variations within the same bone for numerical models. Additional studies are needed to assess the relationship between possible changes of failure strength with donor age.

6. References

1. Ritchie, R. O.; Kinney, J. H.; Kruzic, J. J.; Nalla, R. K. A Fracture Mechanics and Mechanistic Approach to the Failure of Cortical Bone. *Fatigue and Fracture Engineering Materials and Structures* **2005**, *28*, 345–371.
2. Zimmermann, E. A.; Schaible, E.; Bale, H.; Barth, H. D.; Tang, S. Y.; Reichert, P.; Busse, B.; Alliston, T.; Ager, J. W., III; Ritchie, R. O. Age-Related Changes in the Plasticity and Toughness of Human Cortical Bone at Multiple Length-Scales. *Proceedings of the National Academy of Sciences (PNAS)*, August 2011; Vol. 108, pp 14416–14421.
3. Launey, M. E.; Buehler, M. J.; Ritchie, R. O. On the Mechanistic Origins of Toughness in Bone. *Annual Review of Materials Research* **2010**, *40*, 25–53.
4. Gunnarsson, C. A.; Sanborn, B.; Foster, M.; Moy, P.; Weerasooriya, T. Initiation Fracture Toughness of Human Cortical Bone as a Function of Loading Rate. *Proceedings of the SEM International Conference and Exposition on Experimental and Applied Mechanics*, Costa Mesa, CA, 11–12 June 2012.
5. McElhaney, J. Dynamic Response of Bone and Muscle Tissue. *Journal of Applied Physiology* **1966**, *21*, 1231–1236.
6. McElhaney, J.; Fogle, J.; Byars, E.; Weaver, G. Effect of Embalming on the Mechanical Properties of Beef Bone. *Journal of Applied Physiology* **1964**, *19* (6), 1234–1236.
7. Ohman, C.; Dall’Ara, E.; Baleani, M.; Van Sint Jan, S.; Viceconti, M. The Effects of Embalming Using a 4% Formalin Solution on the Compressive Mechanical Properties of Human Cortical Bone. *Clin Biomech. (Bristol, Avon)* **2008**, *23*, 1294–1298.
8. Tennyson, R. C.; Ewert, R. Niranjana, V. Dynamic Viscoelastic Response of Bone. *Experimental Mechanics* **1972**, *12*, 502–507.
9. Lewis, J. L.; Goldsmith, W. A Biaxial Split Hopkinson Bar for Simultaneous Torsion and Compression. *Rev. Sci. Instrum.* **1973**, *44*, 811–813.
10. Lewis, J. L.; Goldsmith, W. The Dynamic Fracture and Prefracture Response of Compact Bone by Split Hopkinson Bar Methods. *J. Biomechanics* **1975**, *8*, 27–40.
11. Ntim, M. M.; Bembey, A. K.; Ferguson, V. I.; Bushby, A. J. Hydration Effects on the Viscoelastic Properties of Collagen. *MRS Proc.* **2006**, *898E*, 39–43.

12. Yamashita, J.; Furman, B. R.; Rawls, H. R.; Wang, X.; Agrawat, C. M. The Use of Dynamic Mechanical Analysis to Assess Viscoelastic Properties of Human Cortical Bone. *Journal of Biomedical Materials Research* **2001**, *58*, 47–53.
13. Katsamais, F.; Raftopoulos, D. Determination of Mechanical Properties of Human Femoral Cortical Bone by the Hopkinson Bar Stress Technique. *Journal of Biomechanics* **1990**, *23* (11), 1173–1184.
14. Tanabe, Y.; Tanaka, S.; Sakamoto, M.; Hara, T.; Takahashi, H.; Koga, Y. Influence of Loading Rate and Anisotropy of Compact Bone. *Journal De Physique III* **1991**, *1*, C3-305-310.
15. Adharapurapu, R. R.; Jiang, F.; Vecchio, K. S. Dynamic Fracture of Bovine Bone. *Materials Science and Engineering* **2006**, *C 26*, 1325–1332.
16. Ferreira, F.; Vaz, M. A.; Simoes, J. A. Mechanical Properties of Bovine Cortical Bone at High Strain Rate. *Materials Characterization* **2006**, *57*, 71–79.
17. Lee, O. S.; Park, J. S.; Dynamic Deformation of Bovine Femur Using SHPB. *Journal of Mechanical Science and Technology* **2011**, *25* (9), 2211–2215.
18. Chen, W.; Song, B. *Split Hopkinson (Kolsky) Bar*; Springer: New York, 2010; pp 29–77.
19. Kulin, R. M.; Jiang, F.; Vecchio, K. S. Effects of Age and Loading Rate on Equine Bone Failure. *Journal of the Mechanical Behavior of Biomedical Materials* **2011**, *4*, 57–75.
20. Parish, A.; Chen, W.; Weerasooriya, T. High Strain Rate Tensile Behavior of Pig Bones. *DYMAT 2009 - 9th International Conference on the Mechanical and Physical Behaviour of Materials Under Dynamic Loading*, Brussels, Belgium, 7–11 September 2009; Vol. 1, pp 917–922.
21. Herwig, K. High Rate Properties of Porcine Skull Bone Tissue. Master's Thesis, Purdue University, West Lafayette, IN, 2010.
22. Reilly, D. T.; Burstein, A. H. The Elastic and Ultimate Properties of Compact Bone Tissue. *Journal of Biomechanics* **1975**, *8* (6), 393–405.
23. Martin, R. B.; Burr, D. B. *Skeletal Tissue Mechanics*; Springer-Verlag: NY, 1998.
24. Gustafson, M. B.; Martin, R. B.; Gibson, V.; Storms, D. H.; Stover, S. M.; Gibeling, J.; Griffin, L. Calcium Buffering Is Required to Maintain Bone Stiffness in Saline Solution. *Journal of Biomechanics* **1996**, *29* (9), 1191–1194.
25. Chu, T. C.; Ranson, W. F.; Sutton, M. A.; Peters, W. H. Applications of Digital-Image-Correlation Techniques to Experimental Mechanics. *Experimental Mechanics* **September 1995**, *25* (3), 232–244.

26. Sutton, M. A.; Wolters, W. J.; Peters, W. H.; Ranson, W. F.; McNeill, S. R. Determination of Displacements Using an Improved Digital Image Correlation Method. *Image and Vision Computing* **1983**, *1* (3), 133–139.
27. Bruck, H. A.; McNeill, S. R.; Russell S. S.; Sutton, M. A. Use of Digital Image Correlation for Determination of Displacements and Strains. In *Non-Destructive Evaluation for Aerospace Requirements*; Workman, G. L., Ed.; Gordon and Breach Science Publishers: Philadelphia, PA, 1989.
28. Sutton, M. A.; McNeill, S. R.; Helm, J. D.; Schreier, H. Full-Field Non-Contacting Measurement of Surface Deformation on Planar or Curved Surfaces Using Advanced Vision Systems. *Proceedings of the International Conference on Advanced Technology in Experimental Mechanics*, July 1999.
29. Chen, W.; Zhang, B.; Forrestal, M. J. A Split Hopkinson Bar Technique for Low Impedance Materials. *Experimental Mechanics* **1999**, *39*, 81–85.
30. Frew, D. J.; Forrestal, M. J.; Chen, W. Pulse Shaping Techniques for Testing Brittle Materials With a Split Hopkinson Pressure Bar. *Exp. Mech.* **2002**, *42*, 93–106.
31. Ko, R. The Tension Test Upon the Compact Substance of Long Bones of Human Extremities. *J. Kyoto Pref Med Univ.* **1953**, *53*, 503–525.
32. Sedlin, E. D. A Rheological Model for Cortical Bone. *Acta Orthopaedica Scandinavica* **1965**, *83*, 1–78.
33. Abendschein, W.; Hyatt, G. W. Ultrasonics and Selected Physical Properties of Bone. *Clin Orthop. Relat. Res.* **March–April 1970**, *69*, 294–301.
34. Bargren, J. H.; Bassett, C. A. L.; Gjelsvik, A. Mechanical Properties of Hydrated Cortical Bone. *Journal of Biomechanics* **1974**, *7*, 239–245.
35. Burstein, A. H.; Reilley, D. T.; Martens, M. Aging of Bone Tissue: Mechanical Properties. *Journal of Bone and Joint Surgery* **1976**, *58-A* (1), 82–86.
36. Smith, B.; Smith, D. A. Relations Between Age, Mineral Density and Mechanical Properties of Human Femoral Compacta. *Acta Orthop Scand*, **1976**, *47*, 496–502.
37. Lappi, V. G.; King, M. S.; LeMay, I. Determination of Elastic Constants for Human Femurs. *J. Biomech Eng.* **1979**, *101*, 193–197.
38. Ohman, C.; Baleani, M.; Pani, C.; Taddei, F.; Alberghini, M.; Viceconti, M.; Manfrini, M. Compressive Behavior of Child and Adult Cortical Bone. *Bone* **2011**, *49*, 796–776.
39. Choi, K.; Kuhn, J. L.; Ciarelli, M. J.; Goldstein, S. A. The Elastic Moduli of Human Subchondral, Trabecular, and Cortical Bone Tissue and the Size-Dependency of Cortical Bone Modulus. *Journal of Biomechanics* **1990**, *23* (11), 1103–1113.

40. Evans, F. G. *Mechanical Properties and Histological Structure of Human Cortical Bone*; ASME70-WA/BHF-7; American Society of Mechanical Engineers: New York, 1970.
41. Yokoo, S. The Compression Test Upon the Diaphysis and the Compact Substance of the Long Bones of Human Extremities. *J. Kyoto Pref Med. Univ.* **1952**, *51*, 291–313.
42. Evans, F. G.; Lebow, M. Regional Differences in Some of the Physical Properties of Human Femur. *Journal of Applied Physiology* **1951**, *3* (9), 563–572.
43. Orais, A. A. E.; Deuerling, J. M.; Landrigan, M. D.; Renaud, J. E.; Roeder, R. K. Anatomic Variation in the Elastic Anisotropy of Cortical Bone Tissue in Human Femur. *Journal of the Biomechanical Behavior of Biomedical Materials* **2009**, *2*, 255–263.
44. Brown, T. D.; Vrahas, M. S. The Apparent Elastic Modulus of the Juxtarticular Subchondral Bone of the Femoral Head. *J. Orthop. Res.* **1984**, *2* (1), 32–38.
45. Lotz, J. C.; Gerhart, T. N.; Hayes, W. C. Mechanical Properties of Metaphyseal Bone in the Proximal Femur. *Journal of Biomechanics* **1991**, *24* (5), 317–329.
46. Murray, R. P.; Hayes, W. C.; Edwards, W. T.; Harry J. D. Mechanical Properties of the Subchondral Plate and the Metaphyseal Shell. *Transactions of the 30th Orthopedic Research Society Meeting*, Atlanta, GA, 6–9 February 1984; p 197.

NO. OF
COPIES ORGANIZATION

1 DEFENSE TECHNICAL
(PDF) INFORMATION CTR
DTIC OCA

2 DIR USARL
(PDF) IMAL HRA
RDRL CIO LL

1 GOVT PRINTG OFC
(PDF) A MALHOTRA

1 US ARMY ATC
(PDF) TEDT AT SLB
A FOURNIER

1 PURDUE UNIV
(PDF) DEPT OF AERONAUTICS
& ASTRONAUTICS
W CHEN

1 UNIV OF NORTH TEXAS
(PDF) DEPT OF MECHL & ENERGY
ENGRNG
X NIE

2 MASSACHUSETTS INST OF TECHLG Y
(PDF) INST FOR SOLDIER
NANOTECHNOLOGIES
R RADOVITZKY
S SOCRATE

1 HUMAN SYSTEMS DEPT
(PDF) NVL AIR WARFARE CTR
AIRCRAFT DIV
B SHENDER

2 DEPT OF MECHL ENGRNG
(PDF) THE JOHNS HOPKINS UNIV
LATROBE 122
K T RAMESH
V NGUYEN

1 UNIV OF TEXAS AUSTIN
(PDF) AEROSPACE ENGRNG AND ENGRNG
MECHS
K RAVI-CHANDAR

2 JTAPIC PROG OFC
(PDF) US ARMY MEDICAL RSRCH AND
MTRL CMND
MRMC RTB
J USCLOWICZ
F LEBEDA

NO. OF
COPIES ORGANIZATION

1 NVL SURFACE WARFARE CTR
(PDF) CODE 664
P DU DT

1 TARDEC
(PDF) RD TA RS
R SCHERER

1 NATICK SOLDIER RSRCH DEV AND
(PDF) ENGRNG CTR
NSRDEC
AMSRD NSC WS TB
M G CARBONI

6 NATICK SOLDIER RSRCH DEV AND
(PDF) ENGRNG CTR
NSRDEC
RDNS D
M CODEGA
RDNS WPW P
R DILALLA
RNDS TSM
M STATKUS
RDNS WSD B
J WARD
P CUNNIFF
M MAFFEO

2 SOUTHWEST RSRCH INST
(PDF) MECHL AND MTRLS ENGRG DIV
MTRLS ENGRG DEPT
D NICOLELLA
W FRANCIS

1 SANDIA NATL LABS
(PDF) B SONG

1 THE UNIV OF UTAH
(PDF) K L MONSON

1 COLUMBIA UNIV
(PDF) 351 ENGINEERING TERRACE
B MORRISON

1 APPLIED RSRCH ASSOC INC
(PDF) SOUTHWEST DIV
C E NEEDHAM

2 CTR FOR INJURY BIOMECHANICS
(PDF) WAKE FOREST UNIV
J STITZEL
F S GAYZIK

<u>NO. OF</u> <u>COPIES</u>	<u>ORGANIZATION</u>
1 (PDF)	US INFANTRY CTR MTRLS LOG NCO SCI TECHN LGY ADVISOR SOLDIER DIV S VAKERICS
3 (PDF)	NATL GROUND INTLLGNC CTR D EPPERLY T SHAVER T WATERBURY
2 (PDF)	PROG EXECUTIVE OFC SOLDIER K MASTERS J ZHENG
2 (PDF)	SOUTHWEST RSRCH INST T HOLMQUIST G JOHNSON
1 (PDF)	AIR FORCE RSRCH LAB AFRL RWMW B MARTIN
100 (PDF)	DIR USARL RDRL DPW R COATES R SPINK RDRL HRS C W HAIRSTON B LANCE K MCDOWELL K OIE J VETTEL RDRL ROE M D STEPP RDRL ROE N L RUSSELL RDRL SLB A B WARD RDRL SLB W A BREUER N EBERIUS P GILLICH C KENNEDY A KULAGA W MERMAGEN K RAFAELS L ROACH RDRL VTP E CHIN

<u>NO. OF</u> <u>COPIES</u>	<u>ORGANIZATION</u>
	RDRL WM P BAKER R DONEY B FORCH S KARNA J MCCAULEY
	RDRL WML M ZOLTOSKI RDRL WML A W OBERLE RDRL WML F G BROWN RDRL WML G J SOUTH RDRL WML H T EHLERS M FERREN-COKER L MAGNESS C MEYER J NEWILL D SCHEFFLER S SCHRAML B SCHUSTER
	RDRL WMM J BEATTY B DOWDING RDRL WMM A D O'BRIEN E WETZEL RDRL WMM B R CARTER B CHEESEMAN G GAZONAS B LOVE P MOY C RANDOW RDRL WMM C A BUJANDA R JENSEN J LA SCALA RDRL WMM D S WALSH W ZIEGLER RDRL WMM E J LASALVIA P PATEL J SINGH J SWAB RDRL WMM F S GREндаHL E KLIER L KECSKES

NO. OF
COPIES ORGANIZATION

RDRL WMM G
J LENHART
R MROZEK
A RAWLETT
K STRAWHECKER
RDRL WMP
S SCHOENFELD
RDRL WMP B
A DAGRO
A DWIVEDI
A GUNNARSSON
C HOPPEL
M LYNCH
D POWELL
B SANBORN
S SATAPATHY
M SCHEIDLER
T WEERASOORIYA
RDRL WMP C
R BECKER
S BILYK
T BJERKE
J BRADLEY
D CASEM
J CLAYTON
D DANDEKAR
M GREENFIELD
B LEAVY
C MEREDITH
M RAFTENBERG
C WILLIAMS
RDRL WMP D
D KLEPONIS
J RUNYEON
B SCOTT
B VONK
RDRL WMP E
S BARTUS
M BURKINS
D HACKBARTH
RDRL WMP F
A FRYDMAN
E FIORAVANTE
N GNIAZDOWSKI
R GUPTA
R KARGUS
RDRL WMP G
N ELDREDGE
RDRL WMS
M VANLANDINGHAM

NO. OF
COPIES ORGANIZATION

4 DRDC VALCARTIER
(PDF) K WILLIAMS
A BOUAMOUL
L MARTINEAU
D NANDLALL

1 DRDC TORONTO
(PDF) C BURRELL

1 HUMAN PROTECTION AND
(PDF) PERFORM DIV
DEFENCE SCI AND TECHLGY ORGN
DEPT OF DEFENCE
T RADTKE

1 DEFENCE SCI AND TECHLGY ORGN
(PDF) S WECKERT